Inorganic Chemistry

Article

pubs.acs.org/IC

Switchable Magnetism: Neutron Diffraction Studies of the Desolvated Coordination Polymer $Co_3(OH)_2(C_4O_4)_2$

Richard A. Mole,*[,†,‡] Muhammad A. Nadeem,[‡,⊥] John A. Stride,[†,‡] Vanessa K. Peterson,[†] and Paul T. Wood [§]

[†]Australian Nuclear Science and Technology Organisation, Locked Bag 2001, Kirrawee DC, New South Wales 2232, Australia

[‡]Department of Chemistry, University of New South Wales, Sydney, New South Wales 2052, Australia

[§]Department of Chemistry, University of Cambridge, Lensfield Road, Cambridge CB2 1EW, U.K.

[⊥]Department of Chemistry, Quaid-i-Azam University, Islamabad, Pakistan

Supporting Information

ABSTRACT: We report the magnetic structure of the two magnetically ordered phases of $Co_3(OH)_2(C_4O_4)_2$, a coordination polymer that consists of a triangular framework decorated with anisotropic Co(II) ions. Neutron diffraction experiments allow us to confirm that the magnetic behavior changes upon dehydration and reveal the complex phase behavior of this system, relative to the hydrated compound $Co_3(OH)_2(C_4O_4)_2{\cdot}3H_2O$. One phase is shown to display spin idle behavior, where only a fraction of the moments order at intermediate temperatures, while at the lowest temperatures the system orders fully, in this case with a net magnetic moment. This novel magnetic behavior is discussed within the framework of a simple Hamiltonian and representational analysis and rationalizes this multiphase behavior by considering the combination of frustration and anisotropy. The change in behavior on dehydration is also rationalized with respect to the changes in the single-ion anisotropy of the cobalt.

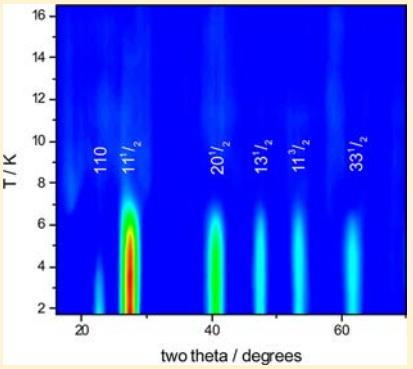

INTRODUCTION

The combination of magnetic or electrical properties with complementary functionalities within a material, so-called multifunctional behavior, is a now well-established methodology in crystal engineering, with many examples in the literature.[1] One notion is the concept of a magnetic sponge:[2] materials that change magnetic properties upon a change of the solvation state. Since the original work on a candidate material, there have been several reports of possible magnetic sponges,[3,4] coinciding with a surge in interest in porous coordination polymers. These novel materials are a major focus in current inorganic materials chemistry research.[5−7] Porous coordination polymers are ideal candidates as magnetic sponges, as paramagnetic transition-metal centers can be readily incorporated into the frameworks and recent reviews have highlighted the continued interest in this area.[8,9] One problem frequently associated with these materials is that use of long ligands as linkers between magnetic centers, as is often the case for porous coordination polymers, runs counter to the conventional wisdom for the rational design of magnetic materials, which requires short linkages for efficient magnetic coupling, while the long bridging pathways common in the structures reported typically have low dimensional magnetic topologies. However, this low dimensionality is itself a key variable in studies of magnetism and low-dimensional materials have allowed the observation of several unusual quantum effects[10,11] which are a rich area for the development of model compounds. The ability to systematically modify exchange and anisotropy contributions in these materials could potentially aid their study and reveal new effects.

One candidate potentially displaying multifunctional behavior is $Co_3(OH)_2(C_4O_4)_2{\cdot}3H_2O$ ($\mathbf{1}{\cdot}3H_2O$).[12] The original report noted the stability of the framework upon dehydration, while subsequent work by Kurmoo et al.[13] reported both the crystal structure of the dehydrated phase $Co_3(OH)_2(C_4O_4)_2$ ($\mathbf{1}$) and some preliminary magnetic susceptibility studies. The reported structural studies highlighted an increase in pore volume upon dehydration, while the magnetic data showed a dramatic change between an antiferromagnetic state and a proposed ferromagnetic state upon dehydration. A subsequent neutron diffraction study of $\mathbf{1}{\cdot}3H_2O$ reported that the magnetic behavior was significantly more complicated,[14] with three predominantly antiferromagnetically ordered phases, one of which showed a novel type of frustrated magnetism called idle spin behavior, another being an antiferromagnetic phase incommensurate to the crystal structure, and the lowest temperature phase having a complicated 90° compromise structure. The neutron diffraction study also confirmed a subtle hydration dependency of the magnetic behavior, where partial dehydration resulted in a different magnetic structure, in contrast to the bulk magnetic data reported previously.[13]

Received: July 16, 2013
Published: November 13, 2013

   dx.doi.org/10.1021/ic4018344 | *Inorg. Chem.* 2013, 52, 13462−13468

Here we extend our previous neutron diffraction study to include the fully dehydrated phase. Although neutron diffraction is an excellent tool for determining structures in systems where there is long-range magnetic ordering and it has long been used in the field of solid-state oxide chemistry, there are comparatively few examples where the magnetic structure has been determined for coordination polymers, although there are an increasing number of reports where this has been applied successfully.[14−20] A relatively recent development is that the problem of deuteration associated with neutron diffraction is not necessarily a limiting restriction when using modern high-flux diffractometers; much of this work has been highlighted in a relatively recent review.[21] As such, neutron diffraction is an ideal counterpart to other more commonly used characterization techniques such as magnetic susceptibility. One of the major advantages of the technique is that the data are typically collected in zero field; therefore, there is no need to consider the added complication of Zeeman splitting. Second, if impurity phases are present in the bulk sample, they can be included quantitatively in the analysis. Finally, the solutions that are obtained from analysis of the neutron diffraction data are the solutions to the Bloch wave functions of the magnetic ground state; these are readily determined by performing the Fourier transform of the real space structure and significantly less likely to result in an incorrect structure determination, in comparison to reports which rely on bulk methods such as susceptibility.

EXPERIMENTAL SECTION

A 0.65 g sample of **1**·3H_2O was prepared using the originally reported synthesis.[12] The sample was placed in a vanadium sample can, equipped with an indium seal and a Swagelock valve. The sample and can were then heated to 100 °C overnight while being evacuated with a turbo pump—consistent with the conditions required for a thorough desolvation as determined by previously reported[12,13] TGA measurements. The can pressure was reduced to a minimum of 4×10^{-6} mbar from the initial value of 1.4×10^{-5} mbar recorded when the turbo pump first achieved full speed. The sample can was then taken into a helium-filled glovebox and the valve replaced with a blanking face.

Neutron diffraction experiments were carried out using the high-intensity powder diffractometer Wombat[22] at The Bragg Institute. The sample was placed in a cryogen-free variable-temperature cryostat (Cryogenic Limited, U.K.) with a single two-stage pulse tube and an external recirculating He loop, allowing a base temperature of 1.6 K to be reached. The sample temperature was measured with a calibrated Cernox sensor. Data were collected in a vanadium can using 2.956(6) Å neutrons achieved using a Ge(113) monochromator as determined using the $La^{11}B_6$ NIST SRM 660b. Wombat features a tertiary-oscillating collimator and an area detector covering 120° in scattering angle (2θ), and data were collected for 10 min over the angular range 15−135°. The data were corrected for detector efficiency and the Debye−Scherrer cones integrated using a standard procedure. All data reduction, correction, and visualization proceedures were undertaken using the program LAMP.[23] Rietveld refinements were performed using the GSAS suite of programs,[24] while the allowed magnetic structures were calculated using the SARAh representational analysis software.[25]

RESULTS

Crystal Structure. The crystal structures of **1**·3H_2O and **1** are already known over a wide temperature range.[12−14] To understand the magnetic behavior of **1**, we need to consider the possible pathways for magnetic superexchange and any differences that occur upon dehydration. The important structural features of **1** and **1**·3H_2O are as follows: μ_3-OH bridged isosceles triangles of cobalt atoms share alternating edges and vertices to form $Co_3(OH)$ strips that lie parallel to the *c* axis and form the backbone of the lattice (Figure 1). Both

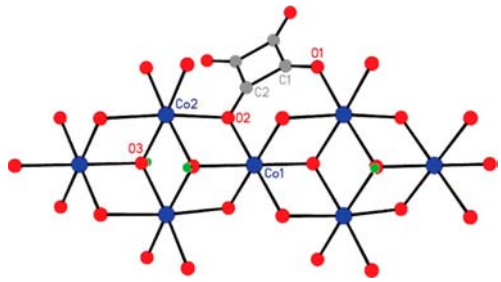

Figure 1. Section of the alternating edge and vertex-sharing chain in **1** (X-ray data reproduced from ref 13), showing the possible bridging interactions.

cobalt ions have a distorted-octahedral coordination environment and are further bridged by squarate dianons via both a one-atom (Co−O−Co) and a four-atom (Co−O−C−C−O−Co) bridge. The squarate dianion also facilitates four- and five-atom bridges to neighboring strips, resulting in the formation of large channels that are occupied with approximately three water molecules in **1**·3H_2O (Figure 2). As shorter superexchange

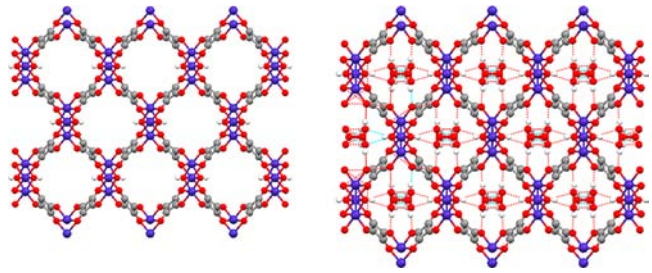

Figure 2. Packing diagrams of **1** and **1**·3H_2O along the crystallographic *c* axis, showing the large water-filled channels and highlighting the lack of major differences in the structure of the framework on dehydration (X-ray data reproduced from ref 13).

pathways typically mediate the strongest spin−spin interactions, it is anticipated that these long bridging pathways between strips will be relatively weak. Upon dehydration of **1**·3H_2O to **1**, there is little change in the framework structure, although an approximately 3.5% increase in the pore volume has been reported,[13] despite the cell volume varying by only approximately 0.5%. The origin of this increase has been reported as being due to the removal of the hydrogen-bonded network of the guest and the host. There are no other major structural changes associated with this increase, and the symmetry of both cobalt sites stays the same. However, there are slight changes in the local coordination environment of the cobalt ions; the scissoring of the cell (reported by Kurmoo et al.) gives rise to a complex displacement, but the changes are at the 1−2% level across all bond lengths and angles.

Previous work[13] has highlighted significant changes in the dc susceptibility on going from the hydrated to the dehydrated phase. The hydrated phase has been thoroughly investigated previously, while the dehydrated phase has only had preliminary susceptibility studies reported. In the dehydrated phase the ac susceptibility shows a broad asymmetric maximum in both χ' and χ'' which has an onset at 8 K and finishes at 5 K, with a maximum at approximately 7 K. The maximum shows a

dx.doi.org/10.1021/ic4018344 | Inorg. Chem. 2013, 52, 13462−13468

variation in intensity with frequency, though there is no variation in peak position. These data imply that there is a phase transition at approximately 8 K and there are no further changes below 5 K

Neutron Diffraction. Inspection of the temperature dependence of the difference patterns (Figure 3) reveals that,

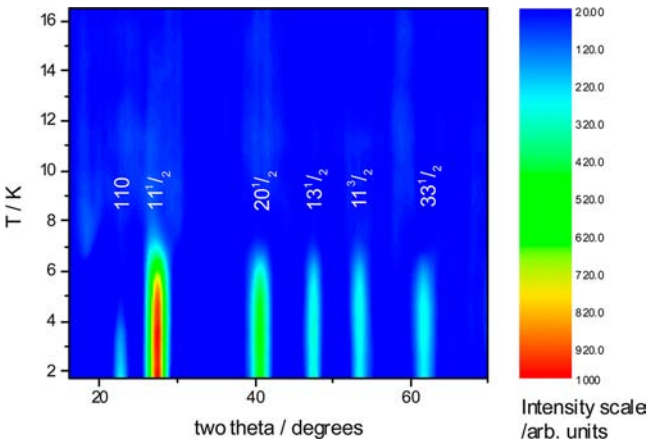

Figure 3. Temperature dependence of the magnetic diffraction in **1**, obtained by subtracting the 16.5 K (well above T_c) diffraction pattern from the data.

at approximately 8 K, extra Bragg reflections are observed, characteristic of a magnetic phase transition. Below 5.75 K, further additional magnetic Bragg peaks are observed. Integrating these Bragg reflections shows a distinct temperature dependence (Figure 4), consistent with two different magnetic phase transitions, in stark contrast with **1**·3H_2O, where three distinct phase transitions were observed.

Attempts to index the magnetic Bragg reflections, observed only below 8 K, revealed a unit cell that is doubled along the *c* axis, indicating possible antiferromagnetic structures and a behavior more complicated than previously hypothesized for

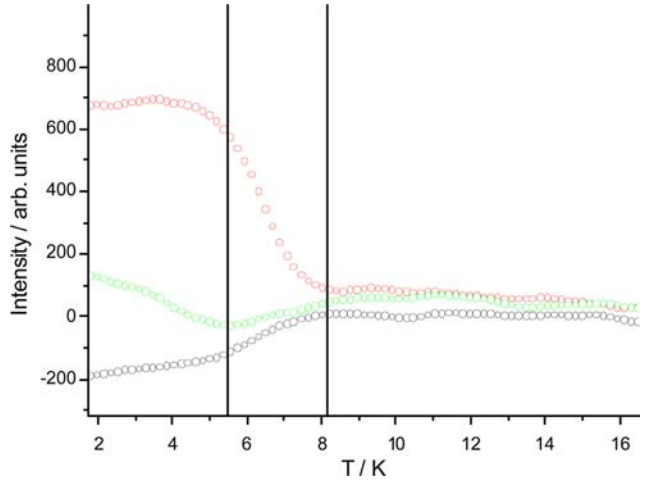

Figure 4. Temperature dependence of the diffraction pattern at several key angles. Red circles are the temperature dependence of the reflection at 27.58°, the green circles 22.75°, and the black circles 33.86°. These are the 110 and the $11^1/_2$ reflections and a background position well away from any Bragg peaks, respectively. The vertical lines at 8 and 5.75 K are the temperatures of the proposed phase changes.

1.[13] The temperature dependence of several Bragg reflections was then determined by integrating each reflection and plotting as a function of temperature (Figure 4), showing several key trends. The $11^1/_2$ reflection is present at 1.6 K and then shows a decrease in intensity until reaching a constant level at 8 K. The 110 reflection is also present at 1.6 K but shows a steady decrease in intensity as the sample is heated, reaching a minimum at 5.75 K. There is a subsequent rise in intensity between 5.75 and 8 K. Finally an integration was taken at 33.68°. This position is free from any Bragg peaks from both the crystal and magnetic structure but is at a sufficiently low 2θ position to be an effective measure of any magnetic contribution to the background, such as diffuse scattering caused by short-range magnetic order. This curve shows a gradual increase upon heating to 5.75 K, at which point a more rapid rise is observed. Above 8 K, the intensity at this position is flat as a function of temperature. One consequence of this change in the fraction of ordered spins contributing to either magnetic Bragg reflections in the ordered phases or diffuse scattering in the paramagnetic phase is that, below 8 K, the background in the difference patterns is negative due to the reduction in magnetic diffuse scattering upon ordering; this effect can be clearly seen in Figures 4 and 5. The observation of

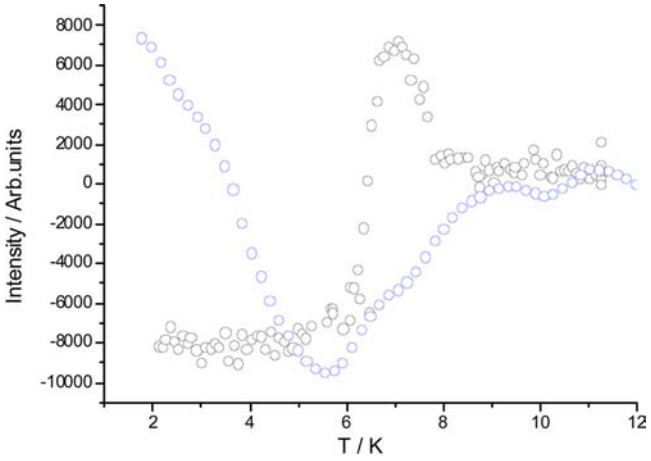

Figure 5. Temperature dependence of the 110 magnetic Bragg reflection for **1** (blue) and **1**·3H_2O (black).

Bragg peaks at two different temperatures is consistent with their being two different phase transitions, while the two-stage change in the magnetic contribution to the background and the rise in intensity of the 110 reflection above 5.75 K are both consistent with a different fraction of the spins being paramagnetic in each temperature region. This is different to the reported data on **1**·3H_2O, where there was no magnetic contribution to the 110 reflection; a similar integration on those data reveals a parasitic contribution from the incommensurate phase (Figure 5) with no other contribution below 6 K. This result shows both the presence of only two phases in **1** and the absence of the incommensurate phase in the dehydrated material and, consequently, that there is a significant variation in the magnetic properties of **1** and **1**·3H_2O.

Initial refinements were performed using the 18 K data, well away from the temperature at which any magnetic phase changes occur. Structural refinements show that the sample is phase pure (Figure 6). The next stage was to determine the magnetic structures at 6 and 1.8 K. To do this, the symmetry-

dx.doi.org/10.1021/ic4018344 | *Inorg. Chem.* 2013, 52, 13462−13468

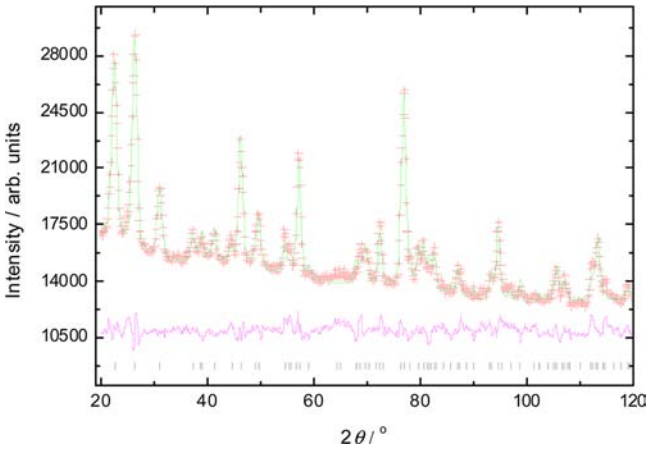

Figure 6. Rietveld refinement using the entire neutron diffraction pattern for **1** at 18 K from the Wombat diffractometer. Black lines indicate allowed positions for Bragg peaks and red crosses the diffraction data. The green line is the calculated diffraction pattern from the proposed structure, and the magenta line is the difference between the calculation and the data.

allowed magnetic structures were determined using the representational analysis technique. This technique allows the magnetic structure to be described in terms of a propagation vector, **k**, and the atomic positions of the magnetic sites. The methods used are described in detail elsewhere,[26−28] and all calculations were performed using the SARAh suite of programs[25] (details of the calculations and each of the allowed structures are given in the Supporting Information). Each predicted structure was trialled in turn and the moment direction determined using a reverse Monte Carlo method.

Refinements were performed on the model at 1.6 K. All Bragg peaks are indexed by the propagation vectors $\mathbf{k} = 10^1/_2$ and $00^1/_2$. The latter must be considered due to the centring of the cell.[26] In both cases, the decompositions of the magnetic representation of the two cobalt atoms Co1 and Co2 are

$$\Gamma_{Co1} = 2\Gamma_2 + 1\Gamma_4$$

$$\Gamma_{Co2} = 1\Gamma_1 + 1\Gamma_2 + 1\Gamma_3 + 1\Gamma_4$$

However, it should be noted that the irreducible representations correspond to different structures for the two propagation vectors. All combinations of propagation vector and irreducible representation were tried, and the moment on each Co ion was refined; the goodness of fit, χ^2, and the magnitude of the moment were noted. None of these trial magnetic structures accurately predict the intensity of the 110 Bragg reflection. As this reflection is coincident with a Bragg peak from the crystal structure, it was initially proposed that this is the ferromagnetic component observed in the work of Kurmoo et al.[13] Subsequent refinements were then made with the propagation vectors Co1 **k** = 000 and Co2 $\mathbf{k} = 00^1/_2$. In this case the irreducible representations transform as follows:

$$\Gamma_{Co1} = \Gamma_1 + 2\Gamma_3$$

$$\Gamma_{Co2} = 1\Gamma_1 + 1\Gamma_2 + 1\Gamma_3 + 1\Gamma_4$$

A summary of these refinements is shown in Table 1.

The best fit to the data was obtained for the following irreducible representations: Co1, $\mathbf{k}_1\ \Gamma_3$; Co2, $\mathbf{k}_2\ \Gamma_1$. There are two basis vectors with Γ_3 symmetry for Co1; these correspond to sublattices with alignment along either the *b* or *c* axis. The orientation of the moment was determined using a reverse Monto Carlo method (Figure 7), which revealed that the moments all lie along the *c* axis. The sublattice of Co2 has only one basis vector, of Γ_1 symmetry; therefore, an equivalent determination of the orientation is unnecessary. The final magnetic structure is shown in Figure 8, taken from the best refinement using the data (Figure 9). This structure has the moment on the vertex sharing site lying along the *c* axis, with all of the moments aligned in parallel—giving a net magnetic moment. Meanwhile the edge-sharing site has the moments on Co2 align coparallel with each other and parallel to the *b* axis along the shared edge, with alternating edges aligned antiparallel to each other. Taking cross sections perpendicular to *c* at, for example, (*h*,*k*,0), (*h*,*k*,0.5), and (*h*,*k*,1) shows that all the Co2 sites have coparallel spins. The magnetic sublattice of the Co2 ions is the same as that observed at low temperatures in $\mathbf{1}\cdot 3H_2O$, while that of Co1 is the same, with the exception that there is now ferromagnetic coupling along the chain as opposed to the antiferromagnetic structure observed previously.

Subsequent refinements were performed on the intermediate temperature phase. The major difference between the low- and intermediate-temperature phases is the observation of the 110 Bragg reflection. As observed in Figure 4, the magnetic contribution to the 110 reflection is no longer present at 6 K; refinements were repeated, without the Co1 **k** = 000

Table 1. Summary of Refinement Data for the Magnetic Structures of 1

Co1 propagation vector and irreducible representation	Co1 moment/ μ_B	Co2 symmetry propagation vector and irreducible representation	Co2 moment/ μ_B	χ^2
$\mathbf{k}_1\ \Gamma_1$	4.64	$\mathbf{k}_2\ \Gamma_1$	3.78	8.453
	4.65	$\mathbf{k}_2\ \Gamma_2$	2.7	9.56
	4.54	$\mathbf{k}_2\ \Gamma_3$	3.54	8.93
	4.36	$\mathbf{k}_2\ \Gamma_4$	2.38	9.98
$\mathbf{k}_2\ \Gamma_3$	5.20	$\mathbf{k}_2\ \Gamma_1$	3.83	8.365
	5.25	$\mathbf{k}_2\ \Gamma_2$	2.76	9.456
	5.37	$\mathbf{k}_2\ \Gamma_3$	3.63	8.779
	5.46	$\mathbf{k}_2\ \Gamma_4$	2.56	9.773

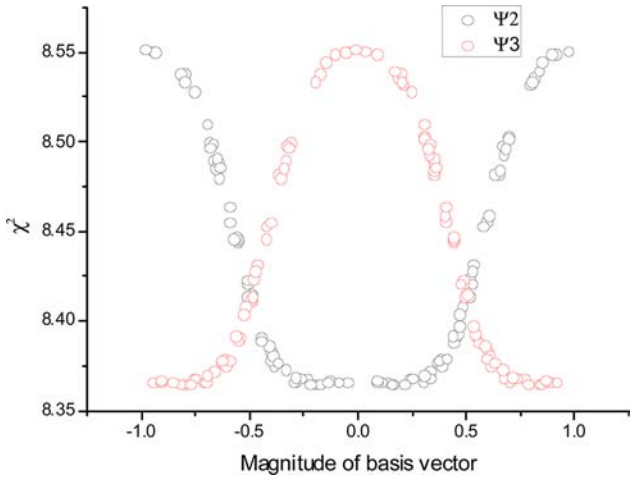

Figure 7. Plot of the goodness of fit, χ^2, for each basis vector Ψ2 and Ψ3. The former corresponds to alignment of the moment along the *b* axis and the latter along the *c* axis.

dx.doi.org/10.1021/ic4018344 | *Inorg. Chem.* 2013, 52, 13462−13468

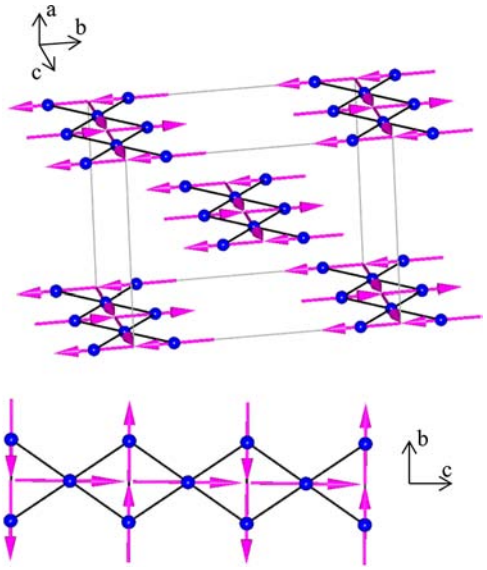

Figure 8. Magnetic structure of **1** determined at 1.8 K.

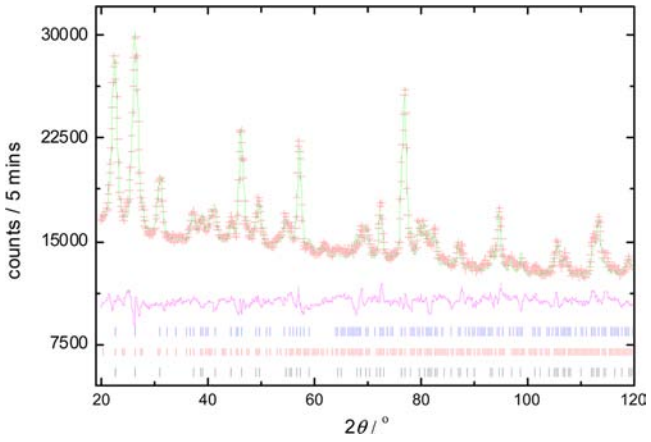

Figure 9. Rietveld refinement using the neutron diffraction data for **1** at 1.8 K. The black tick marks indicate allowed reflections for the crystal structure, the red tick marks the allowed magnetic reflections for Co2, and the blue tick marks the allowed magnetic reflections for Co1. The green line is the calculated diffraction pattern, the red crosses are the observed data points, and the magenta line is the difference between the data and the calculation.

contribution, giving a good fit to the data. The structure observed is the same as the spin idle phase of $\mathbf{1}\cdot 3H_2O$.

Above 8 K, no magnetic Bragg peaks are observed and the data are well described simply by the nuclear crystal structure.

DISCUSSION

The observation of antiferromagnetic reflections automatically precludes the simple explanation of a ferromagnetic phase; however, the neutron diffraction data are not inconsistent with the previously reported susceptibility.[13] One of the key observations of the original work was a switch in the sign of the Weiss constant; this was interpreted as evidence for a change from a simple antiferromagnet to a ferromagnet. Utilizing simple mean field theory, the Weiss constant can be expressed as the sum of the individual exchange interactions; the proposed structure for **1** has more coparallel alignments of spins than $\mathbf{1}\cdot 3H_2O$ when second-nearest-neighbor interactions are included. Assuming that these are all ferromagnetic superexchange interactions (and not some compromise due to the inherent frustration), this could lead to a change of sign for the Weiss constant. Thus, the structure reported here is consistent with the originally reported susceptibility data.

The saturation moment of the dehydrated compound was originally reported as 6 μ_B mol^{-1}, which was thought to be low for three ferromagnetically aligned spins from distorted Co octahedra. The magnetic structure reported here corresponds to 5.2 μ_B mol^{-1}, which is close to the observed value from susceptibility measurements; as described below, this value can be rationalized in terms of the high g factor expected for cobalt(II) in a distorted-octahedral coordination environment, such as that for Co1.

As with $\mathbf{1}\cdot 3H_2O$ the complex magnetic behavior or **1** is thought to arise from the combination of the unquenched orbital angular momentum associated with octahedral Co(II) and the geometric frustration associated with the triangle-based lattice. The same justification for the observation of an idle spin phase can be made here as was previously made for $\mathbf{1}\cdot 3H_2O$.[14] However, there are key differences between the two systems. First, the incommensurate phase is not observed and, second, the fully ordered low-temperature phase shows a net moment. Both of these factors can be explained within the framework of the magnetic anisotropy of the cobalt ions and how small changes in structure affect this.

The spin−orbit coupling associated with the $3d^7$ Co(II) ion in an octahedral coordination environment is known to be strong relative to the crystal field. It is well-known that small distortions of the crystal field can give rise to further increases in the anisotropy.[29] This anisotropy and the associated exchange anisotropy are thought to have strong effects on the observed magnetic properties, though these are often difficult to quantify. Recent work on a series of Co dimers has shown that small structural deviations at the 1−2% level, the same magnitude reported here, can give rise to large changes in the anisotropy of the **g** tensor.[30] The associated changes can then result in significant changes in the magnetic exchange interactions. In the case of cobalt dimers, this resulted in a change from an antiferromagnetic to a ferromagnetic ground state; this was attributed to small structural changes giving rise to a rotation of the **g** tensor, and this subsequently led to differences in the anisotropic exchange interactions. The ultimate result was the switch from ferromagnetic to antiferromagnetic exchange interactions. In the current case a similar mechanism could cause the difference in the magnetic properties of **1** and $\mathbf{1}\cdot 3H_2O$; the variations in the structure of the framework between **1** and $\mathbf{1}\cdot 3H_2O$ are of the same order of magnitude as those observed in ref 30. In particular, there are small changes in the coordination sphere between these two structures and both the magnitude and orientation of the **g** tensor are thought to vary upon dehydration.

The exchange Hamiltonian that was used to describe the magnetic structures of $\mathbf{1}\cdot 3H_2O$ is also a valid starting place for describing the properties of **1**

$$\hat{H} = -J_1 \sum_i S2_i \cdot S2_{i+1} - J_2 \sum_i (S1_i \cdot S2_i + S1_i \cdot S2_{i+1}) + \sum_i (D_1 S1_i^2 + D_2 S2_i^2)$$

where J_1 is the superexchange between Co2 and its symmetry equivalent and J_2 is the superexchange between Co1 and Co2, while S1 and S2 are the spins and D_1 and D_2 are the

dx.doi.org/10.1021/ic4018344 | Inorg. Chem. 2013, 52, 13462−13468

anisotropies associated with Co1 and Co2, respectively. This Hamiltonian does not include any next-nearest-neighbor contributions though, as these require long bridging pathways, it is anticipated that these will only act as minor perturbations.

To be consistent with the analysis of $\mathbf{1}\cdot 3H_2O$,[14] first we should review the number of phases that are observed: in the case of **1**, there are only two phases observed, as opposed to the three observed for $\mathbf{1}\cdot 3H_2O$. There are two limiting cases proposed within representational analysis:[31] $D > J$ and $D < J$. In the first case the two Co sites will behave independently and consequently the ordering of the individual sites does not have to be described by the same irreducible representation and there is no constraint for the sites to order at the same temperature. In the second case there is strong coupling between the Co sites, leading to a single phase transition and a structure where the basis vectors for both spins must belong to the same irreducible representation. In the case of **1**, two phases are observed, indicating that the structures are strongly determined by the anisotropy parameter D; this is different from the case for $\mathbf{1}\cdot 3H_2O$, where three phases are observed due to the fact that D_i and J_i must have similar magnitudes. As such, the differing numbers of phases constitute the first evidence that dehydration results in a change in the anisotropy, while the fact that different irreproducible representations, and in this case different propagation vectors, are observed, adds more weight to the fact that the observed magnetic properties are dominated by the change in anisotropy of the Co ions. To phrase this differently, the observation of two propagation vectors means the magnetic structure of each sublattice is determined by the anisotropy of each cobalt site and that the two sublattices are only weakly coupled.

As with $\mathbf{1}\cdot 3H_2O$, although the structure is based on triangles, the origin of the frustration is not simply antiferromagnetic coupling around the three-membered ring but rather a result of the coupling of the shared edges—with the vertex sharing site unable to satisfy all exchange interactions with either triangle. As a result of this frustration, the observed behavior is of two weakly interacting sublattices. This is reflected in the requirement for two different propagation vectors in the structure solution.

The refined magnitude of the moment is also indicative of this anisotropy. The moment is given by gJ. The $J = {}^1/_2$ term is lowest for octahedral Co(II). The strong anisotropy associated with this term, in particular in the case of distorted coordination environments, can give rise to g factors of up to 13,[29] while for a perfectly octahedral system the g factor is 4.3. The refined moment can be anywhere in the range from 2.15 to 6.5 μ_B, and the change in magnitude of the moments between the hydrated and dehydrated structures is consistent with this complex interplay between the anisotropy of the g factors and the exchange integral.

The measured moment on Co1 changes from 4.00 to 5.20 μ_B on dehydrating $\mathbf{1}\cdot 3H_2O$ to give **1** (corresponding to a change of g from 8 to 10.4), while the moment on Co2 is much smaller, changing from 3.47 to 3.83 μ_B (corresponding to a change in g from 6.94 to 7.66). This suggests that the relatively small change in structure associated with Co2 is not enough to result in changes to the superexchange pathways, while for Co1 the change in the anisotropy is relatively large and the ultimate result is the observation of ferromagnetic coupling between next-nearest neighbors.

CONCLUSION

We have elucidated the nature of the switchable ferromagnetism in the porous coordination polymer $Co_3(OH)_2(C_4O_4)$. This work highlights that neutron diffraction is a powerful tool for this type of work and has shown that the system is significantly more complicated than was originally proposed using susceptibility data alone. Neutron diffraction does, however, only probe the ground states, which provide only an indication of the relative energy scale of the system. Inelastic neutron scattering is a probe that could potentially be used to determine both J and D quantitatively.

The mechanism by which the switchable magnetism occurs is interesting, and there is scope to apply the same methodology to other materials such as sulfur-bridged chains, whereby the superexchange is stronger, and so it may be possible not only to activate such a switching mechanism with dehydration but also to have a higher transition temperature.

The magnetic phase diagram for $Co_3(OH)_2(C_4O_4)\cdot xH_2O$ needs to be elucidated further, particularly with respect to the dependence of the spin idle phase on hydration, where the competition between the ferromagnetic and antiferromagnetic interactions could possibly be tuned to enable the spin idle phase to persist to 0 K. At low temperatures in materials that have allowed the suppression of ordering, novel quantum effects have been observed.[32] There is potential for this material to be a model system for the tuning of the anisotropy in a quantum spin system.

ASSOCIATED CONTENT

Supporting Information

Tables giving the calculated possible magnetic structures determined using representational analysis for $\mathbf{k} = (0,0,0)$, $(1,0,{}^1/_2)$ and $(0,0,{}^1/_2)$ and a CIF file giving crystal data. This material is available free of charge via the Internet at http://pubs.acs.org.

AUTHOR INFORMATION

Corresponding Author

*E-mail for R.A.M.: richard.mole@ansto.gov.au.

Notes

The authors declare no competing financial interest.

ACKNOWLEDGMENTS

We thank the Bragg Insitute (ANSTO) for technical support and J. Leao from the NIST for assistance with sample preparation. M.A.N. was supported by ARC DP0880199 and UNSW FRGP PS27193. R.A.M. thanks UNSW for a visiting fellowship.

REFERENCES

(1) Coronado, E.; Gimenez-Saiz, C.; Marti-Gastaldo, C. In *Engineering of Crystalline Material Properties*; Novoa, J. J., Ed.; Springer: Berlin, 2008; pp 173−191.
(2) Kahn, O.; Larionova, J.; Yakhmi, J. V. *Chem. Eur. J.* **1999**, *5*, 3443.
(3) Ferrando-Soria, J.; Ruiz-Garcia, R.; Cano, J.; Stiriba, S.-E.; Vallejo, J.; Castro, I.; Julve, M.; lloret, F.; Amoros, P.; Pasan, J.; Ruiz-Perez, C.; Journaux, Y.; Pardo, E. *Chem. Eur. J.* **2012**, *18*, 1608.
(4) Wriedt, M.; Yakovenko, A.; Halder, G.; Prosvirin, A.; Dunbar, K. R.; Zhou, H. C. *J. Am. Chem. Soc.* **2013**, *135*, 4040−4050.
(5) Robson, R. *Dalton Trans.* **2008**, 5113.
(6) Cheetham, A. K.; Rao, C. N. R.; Feller, R. K. *Chem. Commun.* **2006**, 4780.

(7) Kitagawa, S.; Kitaura, R.; Noro, S. *Angew. Chem., Int. Ed.* **2004**, *43*, 2334.
(8) Dechambenoit, P.; Long, J. R. *Chem. Soc. Rev.* **2011**, *40*, 3249.
(9) Kurmoo, M. *Chem. Soc. Rev.* **2009**, *38*, 1353.
(10) Jeong, M.; Mayaffre, M, H.; Berthier, C.; Schmidiger, D.; Zheludev, A.; Horvatic, M. *Phys. Rev. Lett.* **2013**, *111*, 6404.
(11) Lake, B.; Tennant, D. A.; Frost, C. D.; Nagler, S. E. *Nat. Mater.* **2005**, *4*, 329.
(12) Gutschke, S. O. H.; Molinier, M.; Powell, A. K.; Wood, P. T. *Angew. Chem., Int. Ed.* **1997**, *36*, 991.
(13) Kurmoo, M.; Kumagai, H.; Chapman, K. W.; Kepert, C. J. *Chem. Commun.* **2005**, 3012.
(14) Mole, R. A.; Stride, J. A.; Henry, P. F.; Hoelzel, M.; Senyshyn, A.; Alberola, A.; Gomez Garcia, C. J.; Raithby, P. R.; Wood, P. T. *Inorg. Chem.* **2011**, *50*, 2246.
(15) Mole, R. A.; Stride, J. A.; Wills, A. S.; Wood, P. T. *Physica B* **2006**, *385*, 435.
(16) Saines, P. J.; Jain, P.; Cheetham, A. K. *Chem. Sci.* **2011**, *2*, 1929.
(17) Feyerherm, R.; Loose, A.; Lawandy, M. A.; Li, J. *J. Phys. Chem. Solids* **2002**, *63*, 71.
(18) Manson, J. L.; Brown, C. M.; Huang, Q.; Schlueter, J. A.; Lancaster, T.; Blundell, S. J.; Singleton, J.; Lynn, J. W.; Pratt, F. L. *Polyhedron* **2013**, *52*, 679.
(19) Saines, P. J.; Yeung, H. H. M.; Hester, J. R.; Lennie, A. R.; Cheetham, A. K. *Dalton Trans.* **2011**, *40*, 6401.
(20) Wang, C. H.; Lumsden, M. D.; Fishman, R. S.; Ehlers, G.; Hong, T.; Tian, W.; Cao, H.; Podlesnyak, A.; Dunmars, C.; Schlueter, J. A.; Manson, J. L.; Christianson, A. D. *Phys. Rev. B.* **2012**, *86*, 064439.
(21) Weller, M. T.; Henry, P. F.; Ting, V. P.; Wilson, C. C. *Chem. Commun* **2009**, 2973.
(22) Studer, A. J.; Hagen, M. E.; Noakes, T. J. *Physica B* **2006**, *385*−*386*, 1013.
(23) LAMP, the Large Array Manipulation Program. http://www.ill.eu/data_treat/lamp/the-lamp-book/.
(24) Larson, A. C.; Von Dreele, R. B. *General Structure Analysis System (GSAS)*; Los Alamos National Laboratory, Los Alamos, NM; Report LAUR 86-748.
(25) Wills, A. S. *Phys. B* **2000**, *276*, 680.
(26) Wills, A. S. *J. Mater. Chem.* **2005**, *15*, 715.
(27) Wills, A. S.; Lappas, A. *J. Phys. Chem. Solids* **2004**, *65*, 65.
(28) Wills, A. S. *Z. Kristallogr.* **2007**, *26* (Suppl), 56.
(29) Abragam, A.; Bleaney, B. I. *Electron Paramagnetic Resonance of Transition Ions*; Oxford University Press: Oxford, U.K., 1970.
(30) Boeer, A. B.; Barra, A.-L.; Chibotaru, L. F.; Collison, D.; McInnes, E. J. L.; Mole, R. A.; Simeoni, G. G.; Timco, G. A.; Ungur, L.; Unruh, T.; Winpenny, R. E. P. *Angew. Chem.* **2011**, *50*, 4007.
(31) Bertaut, E. F. *J. Phys. Colloq.* **1971**, *C1*, 462.
(32) Zheludev, A.; Garlea, O.; Masuda, T.; Manaka, H.; Regnault, L. -P.; Ressouche, E.; Grenier, B.; Chung, J.-H.; Qiu, Y.; Habicht, K.; Kiefer, K.; Boehm, M. *Phys. Rev. B* **2007**, *76*, 054450.